



Article

Unravelling the Crustal Architecture of Cape Verde from the Seamount Xenolith Record

Abigail K. Barker ^{1,2,*} , Thor H. Hansteen ³  and David Nilsson ¹

¹ Mineralogy Petrology Tectonics, Department of Earth Sciences, Uppsala University, Villavägen 16, SE-752 36 Uppsala, Sweden; dnilson@gmail.com

² Centre of Natural Hazards and Disaster Sciences (CNDS), Villavägen 16, SE-752 36 Uppsala, Sweden

³ GEOMAR Helmholtz Centre for Ocean Research Kiel, Wischhofstraße, 1-3, D-24148 Kiel, Germany; thansteen@geomar.de

* Correspondence: abigail.barker@geo.uu.se; Tel.: +46-18-471-2552

Received: 30 December 2018; Accepted: 29 January 2019; Published: 1 February 2019



Abstract: The Cape Verde oceanic plateau hosts 10 islands and 11 seamounts and provides an extensive suite of alkaline lavas and pyroclastic rocks. The volcanic rocks host a range of crustal and mantle xenoliths. These xenoliths provide a spectrum of lithologies available to interact with magma during transport through the lithospheric mantle and crust. We explore the origin and depth of formation of crustal xenoliths to develop a framework of magma-crust interaction and a model for the crustal architecture beneath the Cape Verde oceanic plateau. The host lavas are phononephelinites to phonolites and the crustal xenoliths are mostly mafic plutonic assemblages with one sedimentary xenolith. REE profiles of clinopyroxene in the host lavas are light rare-earth element (LREE) enriched whereas clinopyroxene from the plutonic xenoliths are LREE depleted. Modelling of REE melt compositions indicates the plutonic xenoliths are derived from mid-ocean ridge basalt (MORB)-type ocean crust. Thermobarometry indicates that clinopyroxene in the host lavas formed at depths of 17 to 46 km, whereas those in the xenoliths formed at 5 to 20 km. This places the depth of origin of the plutonic xenoliths in the oceanic crust. Therefore, the xenoliths trace magma-crust interaction to the MORB oceanic crust and overlying sediments located beneath the Cape Verde oceanic plateau.

Keywords: alkaline volcanics; crustal xenoliths; thermobarometry; magma-crust interaction

1. Introduction

The Cape Verde archipelago is a collection of exposed islands and seamounts perched atop a volcanic oceanic plateau. The volcanics are alkaline in nature with some rocks exhibiting feldspathoids and although dominantly mafic a few of the volcanic centres are composed of felsic volcanics [1–4]. The suite of lavas, sampled from the Cape Verde oceanic plateau by the Meteor Expedition M80/3 in January 2010, hosts a range of xenoliths. Crustal xenoliths are key to understanding magma-crust interaction and the crustal architecture beneath Cape Verde. Therefore we focus on crustal xenoliths found in lavas from remotely operated vehicle (ROV) dives and dredges of the Cadamosto Seamount and the Charles Darwin Volcanic Field (Figure 1). The Cadamosto Seamount is a roughly 2000 m high, large, mature dominantly phonolitic seamount [4], whereas the Charles Darwin Volcanic Field is comprised of multiple small, young mafic to phonolitic eruption centres on the Cape Verde plateau.

We present petrography and mineral chemistry including trace element geochemistry for clinopyroxene and thermobarometric modelling. Our objective is to investigate the nature of magma-crust interaction, the origin of the xenoliths and crustal architecture beneath the Cape Verde archipelago in order to understand the magmatic system.

Previous reports of xenoliths from Cape Verde have focused on mantle xenoliths [5], whereas studies of the Canary Islands show a broad range of xenoliths including cumulates from deep within the Ocean Island complex [6,7] and sedimentary crustal xenoliths [8–11]. The sedimentary xenoliths sample the thick pre-existing sedimentary pile beneath the volcanoes [12].

Mineral-melt thermobarometry is widely applied to volcanic systems in order to develop an understanding of the magma plumbing system that feeds volcanoes, for example, [7,13]. Thermobarometric studies of the Cape Verde archipelago have shown that the dominant magma storage zones are deep seated, typically in the upper oceanic lithospheric mantle, below the Moho [3,4,14,15]. Evidence of the shallower magmatic system comes from re-equilibration of fluid inclusions and a touch of assimilation of sedimentary rocks [4,14,15].

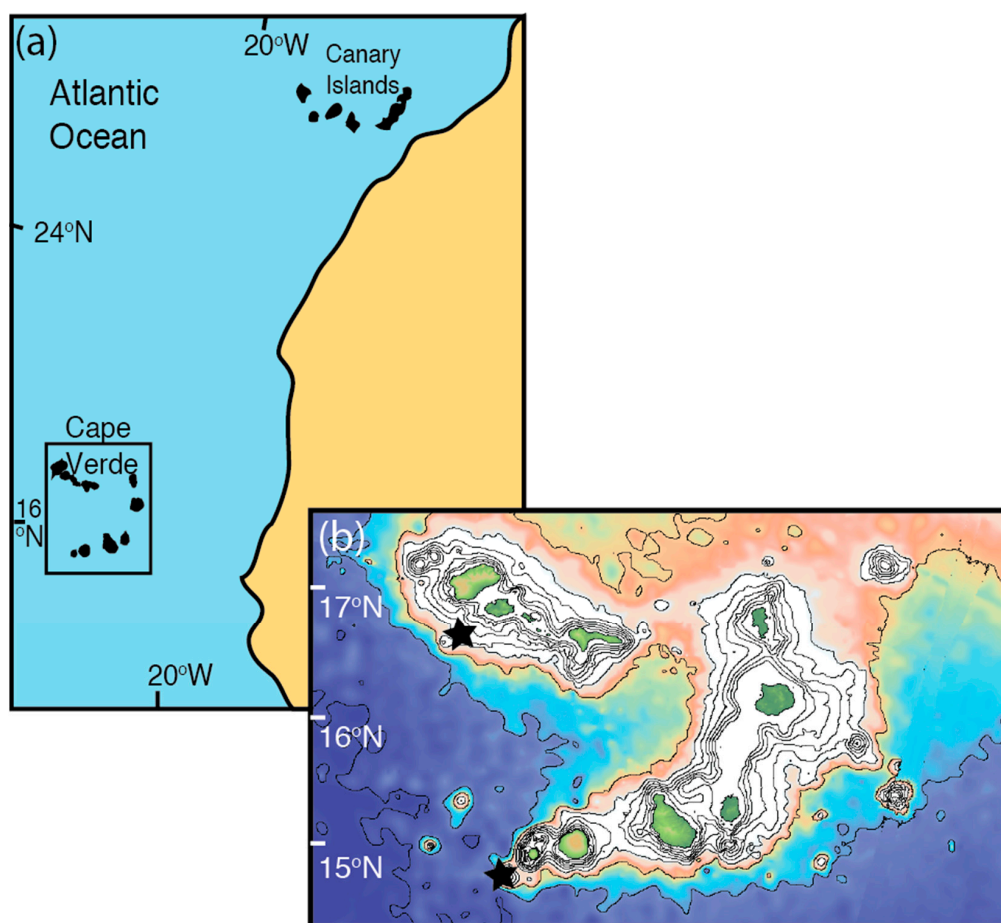


Figure 1. (a) Location map of the Cape Verde archipelago, (b) shows the Cape Verde islands and bathymetry including certain seamounts (credit due to [16]). The oceanic plateau was extensively sampled by ROV dives and dredging during the Meteor M80/3 expedition to Cape Verde in January 2010. The stars mark the locations of xenolith bearing samples featured in this study. The southwestern star depicts the Cadamosto Seamount located at the southwest of the southern chain of volcanic islands. The other star marks the Charles Darwin Volcanic Field, which lies southwest of the northern volcanic island chain, on the lower submarine flank of Santo Antão.

We demonstrate that xenolith mineral reaction rims signal high temperature magma-crust interaction and geochemical mapping demonstrates limited exchange between xenoliths and the host magma. We find from the contrasting petrography between the volcanic host rocks, and xenoliths and also from modelling partitioning of trace elements, that the xenoliths are derived from a MORB-type crust. Integrated with the resulting thermobarometry we demonstrate that the Cape Verde alkaline

magmas collect xenoliths from various depths on ascent through the ocean crust and overlying sedimentary rocks.

2. Materials and Methods

Mineral chemistry analysis was performed by field emission gun JEOL JXA-8530F Hyperprobe at Uppsala University, Uppsala, Sweden. The operating conditions were 10 nA probe current and 15 kV accelerating voltage and the phi-rho-Z (PRZ) correction was employed. Precision of analyses is typically <2.2% s.d. with <4.5% s.d. for Na, see [7] for further details. Data is presented in Supplementary Table S1.

The rare earth elements were measured in clinopyroxene by laser ablation ICP-MS at GEOMAR Helmholtz Centre for Ocean Research Kiel, Kiel, Germany [17], using a 193 nm Excimer laser ablation system (Coherent, GeoLasPro, Santa Clara, CA, USA) coupled to a double-focusing, high-resolution magnetic sector mass spectrometer (Nu Instruments, AttoM, Wrexham, UK). Ablation by 300 pulses at 10 Hz, 32 μm spot size and laser energy density of $4 \text{ J}\cdot\text{cm}^{-2}$ was performed with a He carrier gas. An Ar carrier gas was added after the ablation cell. A gas background of 50 s was collected prior to each ablation. NIST612 and StHs6/80-G glass standards were used for calibration [18,19]. Data is presented in Supplementary Table S2.

The majority of thermobarometric formulations are not calibrated for alkaline systems [13]. Those suitable for alkaline systems focus on ultramafic to mafic assemblages [20]. One formulation exists specifically for evolved alkaline conditions with high $\text{K}_2\text{O}/\text{Na}_2\text{O}$ (1.3 to 2.5; [21]). However, the evolved Cape Verde volcanics have comparatively low $\text{K}_2\text{O}/\text{Na}_2\text{O}$ (0.25 to 0.75) [4], therefore even this formulation is not optimal. Hence, we employ the only suitable thermobarometer calibrated for a wide range of compositions including evolved alkaline conditions [13,22]. Pressures and temperatures of the clinopyroxene from the xenoliths and host lavas were estimated by clinopyroxene-liquid equilibrium thermobarometry following [22], to facilitate inter-comparison between the lavas and xenoliths. In addition, the minerals in the crustal xenoliths were modelled for clinopyroxene crystallization from mineral chemistry only by equation 32c and 32d in Reference [13] and plagioclase-liquid thermobarometry of Reference [23] was applied to plagioclase from the xenoliths. These thermobarometric models perform with uncertainties of $\pm 33^\circ\text{C}$ and $\pm 0.17 \text{ GPa}$ for clinopyroxene-liquid [22]; $\pm 58^\circ\text{C}$ and $\pm 0.15 \text{ GPa}$ for single clinopyroxene and $\pm 36^\circ\text{C}$ and $\pm 0.25 \text{ GPa}$ for plagioclase-liquid [13]. In the absence of groundmass glass and given the unreliability of melt inclusions [24], suitable nominal liquids to pair with the minerals were chosen based on Fe-Mg partitioning and clinopyroxene components or An-Ab partitioning for clinopyroxene and plagioclase respectively (Figure S1). Only the data that show equilibrium in Fe-Mg and clinopyroxene components were used to conduct thermobarometry. For clinopyroxene in the lavas, whole rock compositions with Mg# 46 to 50 were selected [25]. Notably clinopyroxene crystallizing at olivine contacts with the xenoliths are in equilibrium with a whole rock composition of Mg# 38. The majority of the clinopyroxene crystals fall within the $K_D(\text{Fe-Mg})^{\text{cpx-liq}}$ of 0.275 ± 0.067 [22] and also the equilibrium envelopes for clinopyroxene components [13](Figure S1). We assume that the minerals in the xenoliths either grew during fractional crystallization and separated from the melt to form cumulates or formed under equilibrium crystallization conditions. Therefore, the xenoliths were matched with whole rock MORB compositions from the Central Atlantic. The clinopyroxene in the xenoliths was determined to be in equilibrium with sample compositions of 50.5 to 58.5 Mg# and 51.7 to 52.5 wt. % SiO_2 [26] by Fe-Mg partitioning and clinopyroxene components (Figure S1). In turn, the plagioclase crystals in the xenoliths were found to be in equilibrium with a sample of Atlantic MORB with 50.1 wt. % SiO_2 with water content of 0% [27] (Figure S1).

The Cape Verde volcanics are relatively oxidized with $\text{Fe}^{3+}/\text{Fe}^{\text{total}}$ of 0.19 to 0.26 for Santa Antão and Sao Nicolai [25,28]. This is confirmed by oxygen fugacity of -0.6 to $+2.2 \log \Delta\text{QFM}$ for ultramafic xenoliths from Cape Verde [29]. The relatively oxidized nature of magmas from the Cape Verde archipelago is consistent with reports of Ocean Island Basalt at $\text{Fe}^{3+}/\text{Fe}^{\text{total}}$ of 0.15 to 0.25 [30]. We therefore performed the clinopyroxene-liquid thermobarometry with $\text{Fe}^{3+}/\text{Fe}^{\text{total}}$ of 0.21 for the nominal liquid.

3. Results

3.1. Host Lavas

The lavas found to carry xenoliths are relatively evolved for lavas from Cape Verde, being phononephelinite to phonolite in nature [1–4,14,15,25,31,32]. Whole rock compositions for lavas from the Cadamosto Seamount display Mg# of 29–37 [4]. The host rocks are porphyritic lavas that contain nosean, nepheline, pyroxene (diopside and aegirine), biotite and minor apatite, sanidine and iron oxide phenocrysts with fine grained to glassy groundmass (Figure 2A,B and Figure 3). Diopside to augite ($\text{Wo}_{43-48}\text{En}_{33-43}\text{Fs}_{12-20}$) in the lavas has Mg# of 62 to 78 ($n = 54$; Figure 3) and sanidine is sodium-sanidine at Or_{63} ($n = 2$; Figure 3). Clinopyroxene in the lavas shows slightly enriched LREE and almost flat heavy rare-earth elements (HREE) (Figure 4a).

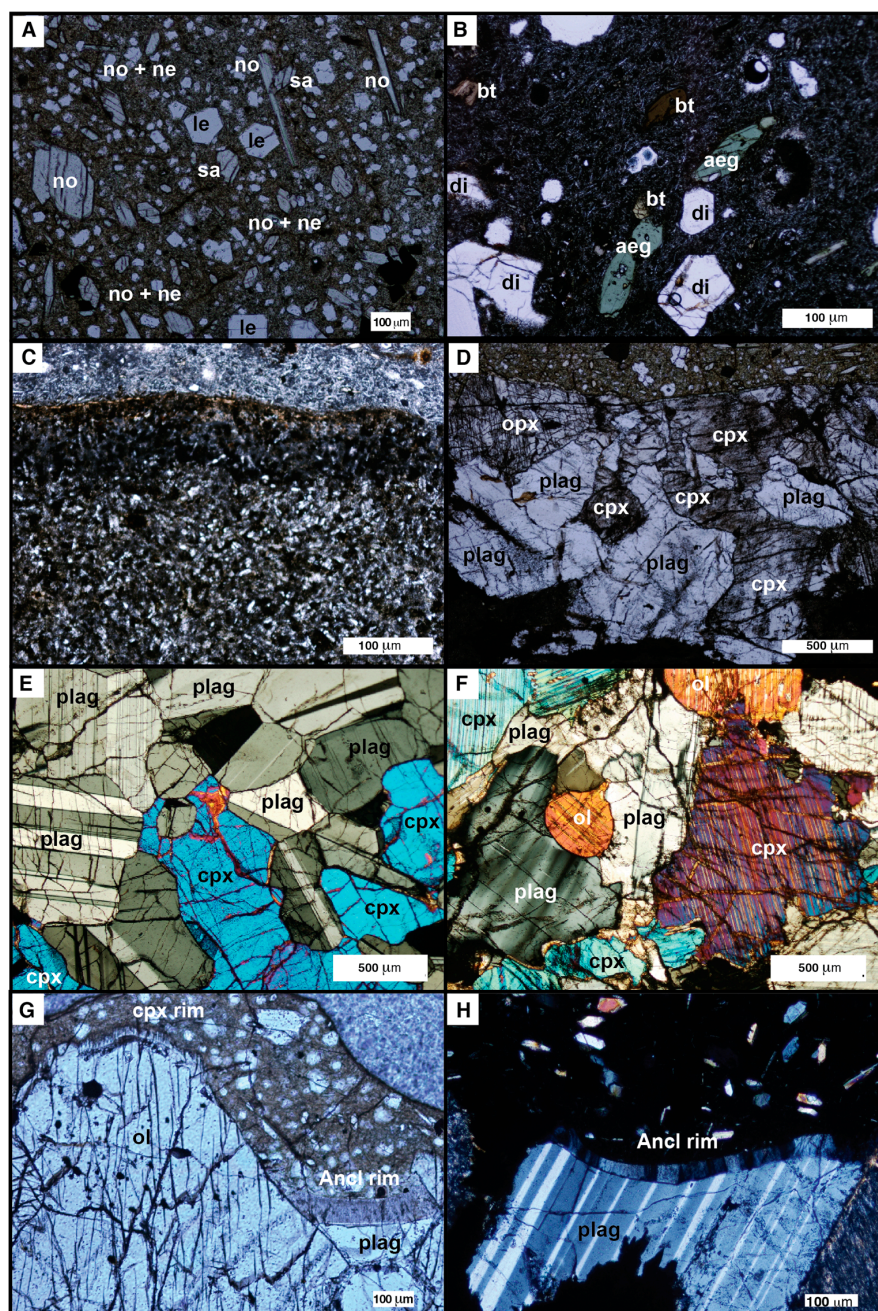


Figure 2. Photomicrographs of host lavas and xenoliths from Cape Verde.

(A) Feldspathoids in a lava from the Charles Darwin Volcanic Field (Sample 068DR14). (B) Phononephelinite from the Cadamosto Seamount (Sample 035ROV10). (C) Sedimentary xenolith with fine grained detrital quartz, feldspar and biotite in a clay matrix. Note the 100 μm contact zone with the lava. (Sample 035ROV10). (D) Clinopyroxene, orthopyroxene and plagioclase bearing gabbro xenolith (Sample 068DR03). (E) Plagioclase and clinopyroxene in a gabbro xenolith (Sample 067ROV07) (XPL) (F) Olivine, clinopyroxene and plagioclase in a gabbro xenolith (Sample 068DR03) (XPL). (G) Xenolith contact with narrow rim on olivine and wide (100 μm) rim on plagioclase (Sample 068DR14). (H) Finely recrystallized anorthoclase rim on xenolith plagioclase (Sample 068DR03) (XPL). Abbreviations: plag—plagioclase, ol—olivine, opx—orthopyroxene, cpx—clinopyroxene, di—diopside, aeg—aeirine, bt—biotite, no—nosean, ne—nepheline, le—leucite, sa—sanidine, ancl—anorthoclase.

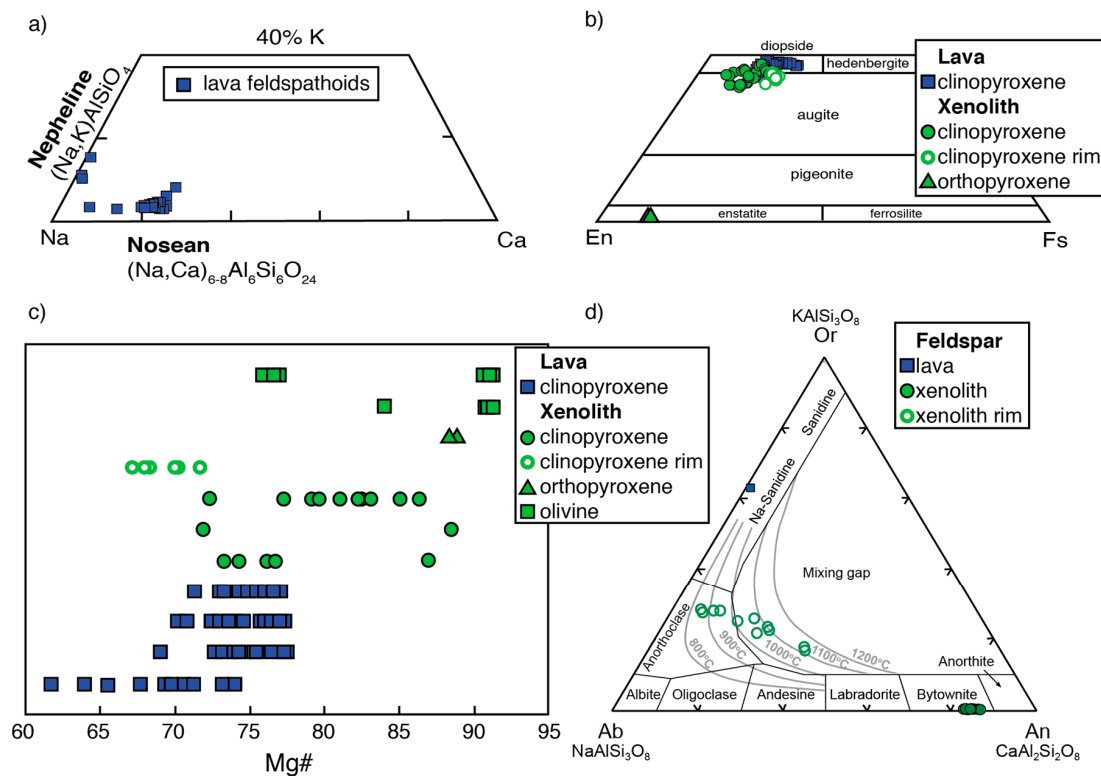


Figure 3. Mineral chemistry classification: (a) The feldspathoids found in the lavas classify as nosean and nepheline; (b) The lavas host diopside, whereas the xenoliths host both diopside-augite and enstatite; (c) Mg# for clinopyroxene in lavas and clinopyroxene, orthopyroxene and olivine in xenoliths; (d) Rare Na-sanidine is found in the lavas while the xenoliths are rich in anorthitic plagioclase, whereas the reaction rim is anorthoclase in composition. The ternary diagram features isotherms from [33]. Credit is given to Delta-plot for ternary plots.

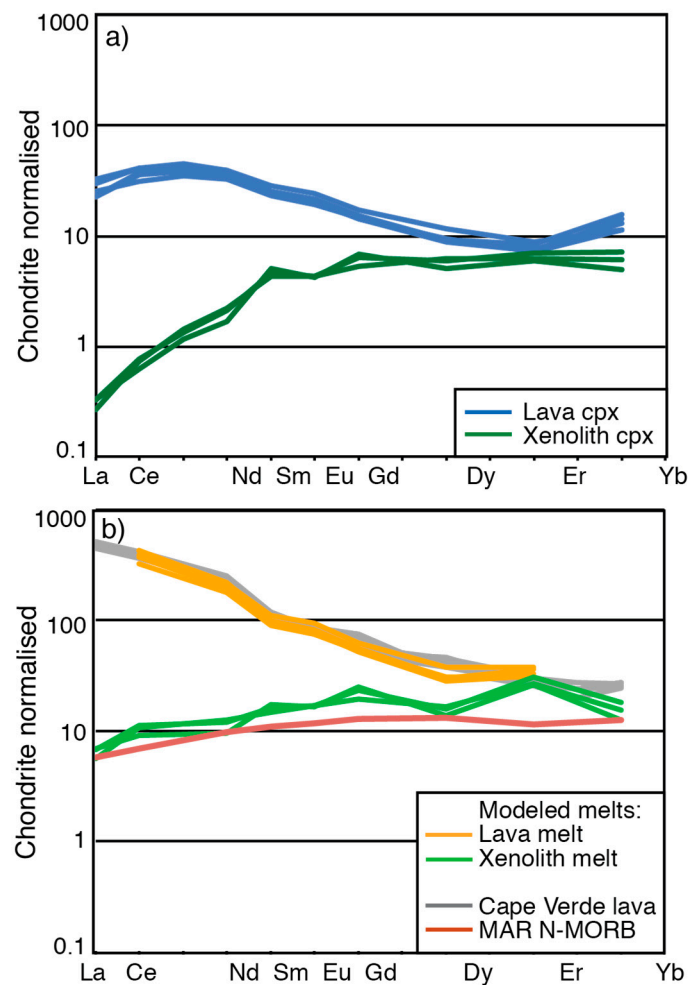


Figure 4. REE profiles for clinopyroxene from the xenoliths and host lavas. (a) The clinopyroxene in the lavas is slightly enriched in LREE whereas the xenoliths have clinopyroxene with depleted LREE. (b) Modelling has been undertaken to determine corresponding melts associated with clinopyroxene to compare with the Cape Verde OIB source and MORB [4,34]. Partition coefficients used in modelling are taken from [35] for the Cape Verde nephelinitic to phonolitic lavas and [36] for the gabbro xenoliths.

3.2. Xenoliths

The crustal xenoliths are on the order of a few centimetres ranging from 1 to 5 cm by <0.5 to 2 cm. A single fine grained xenolith contains detrital quartz, feldspar and biotite in a matrix of clay and displays primary layering (Figure 2C). A 100 μm reaction zone with the magma is finer grained and clay rich and the last few microns display iron staining. The other xenoliths are mafic plutonic lithologies ($n = 8$) composed of plagioclase, clinopyroxene, olivine and orthopyroxene crystals (100 μm), which form an equigranular texture (Figure 2D–F). Xenolith plagioclase has An of 83 to 87 ($n = 34$), olivine has Fo contents of 74 to 91% ($n = 27$), orthopyroxene has En 88–89% ($n = 4$) and clinopyroxene is augite to diopside ($\text{Wo}_{40-47}\text{En}_{40-50}\text{Fs}_{7-16}$) with Mg# 72 to 88 ($n = 20$; Figures 2 and 3). Clinopyroxene in the xenoliths has highly depleted LREE patterns in contrast to those in the lavas but similar flat and slightly more depleted HREE patterns (Figure 4a).

The reaction zones on plagioclase feldspar are 30 to 100 μm , where the rim is finely recrystallized anorthoclase ($\text{An}_{7-36}\text{Ab}_{45-65}\text{Or}_{17-29}$; Figure 2G,H and Figure 5), whereas reaction zones juxtaposed against subrounded olivine crystals are ca. 10 μm where the rim composition is augite ($\text{Wo}_{41-45}\text{En}_{38-42}\text{Fs}_{16-19}$; Figures 2G, 3 and 4). One mafic plutonic xenolith shows a finely recrystallized groundmass of olivine (Fo 81), phlogopite and clinopyroxene (augite Mg# 86).

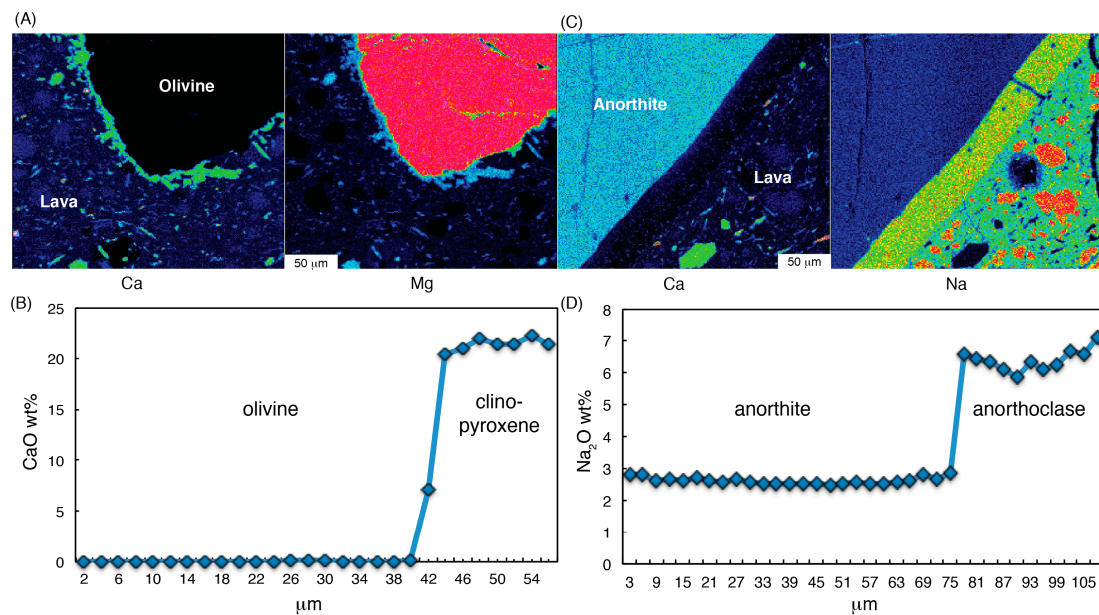


Figure 5. WDS element maps and geochemical traverses showing xenolith-magma contacts. (A,B) Olivine lacking Ca with high Mg has a 12 μm contact zone of clinopyroxene with high Ca and low MgO due to crystallization from the host magma. (C,D) Anorthitic plagioclase with high Ca and low Na content against the high Na and low Ca host lava. The 50 μm contact zone has transformed to anorthoclase with low Ca and very high Na and displays a finely recrystallized texture.

4. Discussion

4.1. Magma-Crust Interaction

The presence of the xenoliths indicates a role for magma-crust interaction on a limited timescale such that the xenoliths do not completely breakdown. Such crustal xenoliths may either originate as wall rocks of magma chambers or be incorporated during rapid magma ascent through feeder dykes, for example, [37]. Additionally, the reaction zones on the xenoliths record the thermal conditions of the interaction with the magma and hence reveal the processes of magma-crust interaction.

The petrography and mineral chemistry of gabbroic xenoliths show two types of reaction zones: 1) finely recrystallized anorthoclase rims of 30 to 100 μm width on plagioclase and 2) heterogeneous clinopyroxene overgrowths on subrounded olivine in a ca. 10 μm wide zone (Figures 2, 3 and 5). Furthermore, the element mapping suggests the magma-rock interaction predominantly affects the xenoliths, with no geochemical gradients appearing in the groundmass of the host lava (Figure 5).

On initial contact with the magma, olivine grains at the surface of the gabbro xenoliths begin to dissolve and olivine at the contact becomes subrounded [38]. Subsequently olivine acts as a nucleation surface for clinopyroxene crystals that grow from the melt [39]. These small randomly oriented clinopyroxene crystals attach to the olivine protecting the olivine from further reaction with the melt (Figure 5) [6]. Variations in the thickness of the rim and size of the clinopyroxene crystals likely represent compositional heterogeneity of the proximal melt. Clinopyroxene-melt thermometry has been applied to the clinopyroxene reaction rims giving a temperature estimate of 1005 ± 10 °C 1s.d. ($n = 6$) [13,22]. The temperature derived for the clinopyroxene xenolith rims is slightly lower than the host magma temperature of 1083 ± 63 °C 1s.d. ($n = 54$) [13,22]. These temperature estimates indicate clinopyroxene rim crystallization at magmatic temperatures and are consistent with the cooling of the magma during ascent. Additionally, the clinopyroxene rim chemistry is similar to the composition of the clinopyroxene from the lavas. The clinopyroxene rim compositions extend to lower Mg# and CaO content and higher TiO_2 , Al_2O_3 and Na_2O content consistent with rim growth in a more evolved and cooler magma.

In contrast, the rim of the xenolith plagioclase undergoes incongruent melting as it becomes heated through contact with the hot magma [40]. The melt produced by the incongruent plagioclase melting will be relatively Na-rich compared to the original mineral. Additionally, the host magma is phonolitic in composition and the feldspar in equilibrium with the melt is sanidine (Figure 3). Therefore, mingling between the host magma and plagioclase partial melt at the surface of the xenolith will result in anorthoclase growth at the respective interface (Figure 3). The conditions of anorthoclase formation can be estimated by comparison with isotherms and suggest growth at 800 °C to 1150 °C (Figure 3) [33]. Further evidence of partial melting and mingling of melts is the very finely recrystallized texture that suggests rapid cooling of the anorthoclase (Figure 2H). Incomplete mingling between the host magma and plagioclase partial melt also accounts for the heterogeneity of Or and Ab in the anorthoclase (Figure 5).

Thus, the two different mechanisms occurring at magmatic temperatures support the observations of variations in thickness of the melt reaction zones (Figure 5).

4.2. Origin of Xenoliths

The xenoliths sampled by the ascending magmas provide a record of the crustal lithologies the melts have passed through. We draw on petrography and mineral chemistry to decipher the origin of the xenoliths and thermobarometric modelling to determine crystallization depths for the xenolith precursor magmas. Integrating the information derived on the origin and depth of formation of the xenoliths we build up a model for the architecture of the crust beneath the Cape Verde archipelago and thus the submarine volcanic plateau.

The Cape Verde magmatism is highly silica undersaturated with basanites, nephelinites and mela-nephelinites forming the typical mafic volcanic products [1–3,25,32]. When such a system evolves to produce felsic end-members a highly alkaline trend is followed, leading to phonolites that are devoid of silica oversaturated phases such as quartz and favouring alkali feldspar over plagioclase [4,14,15,25,41].

The mafic plutonic xenoliths contrast in mineralogy to the host lavas in terms of the presence of anorthitic plagioclase associated with silica-saturated tholeiitic gabbro lithologies. Thus they contrast with the feldspathoids and alkali feldspar found in the host lavas and more generally in Cape Verde lavas suggesting a different origin (Figures 2, 3 and 5), for example, [1–3,25,32,42].

Further evidence of the contrast in origin of the mafic plutonic xenoliths and host lavas is found in the REE compositions of the clinopyroxene. The xenoliths display depleted LREE patterns whilst clinopyroxene in the lavas have slightly enriched LREE (Figure 4a). Using partition coefficients from [35,36] to calculate the associated melt composition we find that the xenoliths are derived from a melt with a slightly LREE-depleted source, comparable to a Mid Atlantic Ridge Basalt, whereas the clinopyroxene hosted by the lavas reflect melt compositions with enriched LREE's corresponding to felsic Cape Verde lavas (Figure 4b). Integration with petrological information indicates that the xenoliths are gabbro derived from the pre-island ocean crust whereas the lavas are consistent with the Cape Verde hotspot activity.

Moreover clinopyroxene from the lavas crystallized at pressures of 0.4 to 1.2 GPa. Taking the uncertainties of ± 0.17 GPa into account, these pressures correspond to depths near and below the Moho and therefore represent crystallization in the oceanic lithospheric mantle (Figure 6). These crystallization conditions are consistent with other studies on clinopyroxene from Cape Verde [3,4,14,15]. In contrast, plagioclase from the mafic plutonic xenoliths formed at pressures of 0.1 to 0.3 GPa, with an uncertainty of ± 0.25 GPa. Likewise the majority of the clinopyroxene crystallized between 0.1 and 0.6 GPa. These pressure estimates are associated with uncertainties of ± 0.15 and ± 0.17 GPa for single clinopyroxene and clinopyroxene-liquid thermobarometers, respectively. Hence the clinopyroxene and plagioclase crystallization pressures for the xenoliths indicate shallower depths of formation, within uncertainty of the lower ocean crust (Figure 4) [43]. This once again

confirms the different origin of the lavas and mafic plutonic xenoliths consistent with an ocean crust origin for the gabbro xenoliths.

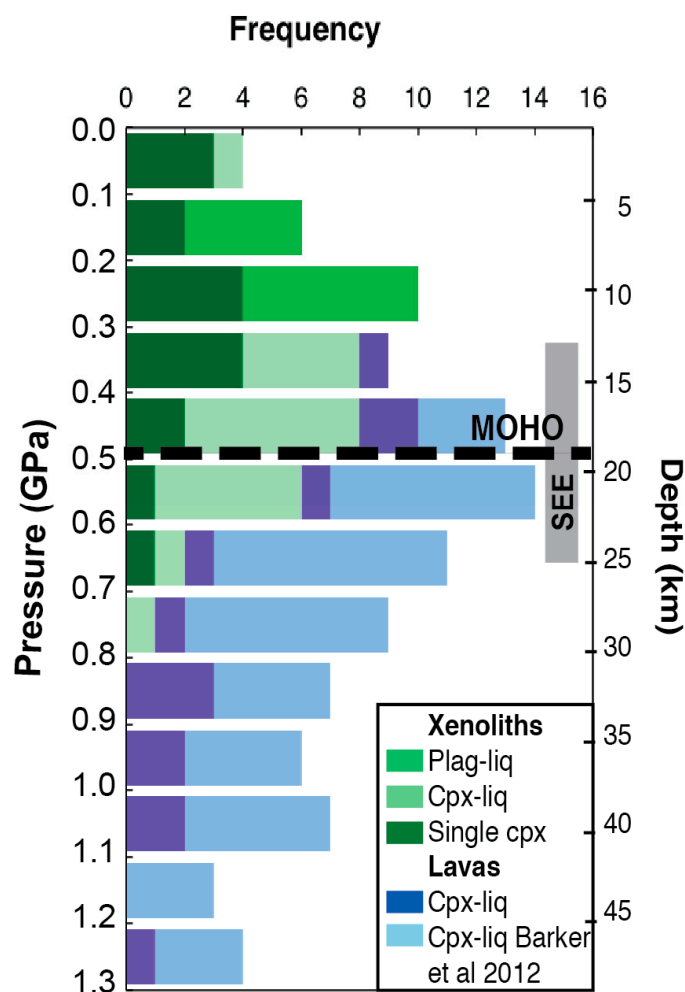


Figure 6. Pressure and depth profile for clinopyroxene and plagioclase from lavas and xenoliths from Cape Verde. Clinopyroxene-melt, single clinopyroxene and feldspar-melt thermometers were used for thermobarometric calculations [13,22,23]. Clinopyroxene crystallization in the lavas occurred dominantly at pressures of ≥ 0.5 GPa, originating from below the Moho, hence crystallization of the lavas occurred in the oceanic lithospheric mantle [4]. The majority of clinopyroxene and plagioclase in the xenoliths crystallized between 0.2 and 0.4 GPa, above the Moho in the oceanic crust. The Moho was determined to be 18 ± 1 km at Cape Verde [43]. The uncertainty for clinopyroxene-liquid pressure estimates is ± 0.17 GPa (standard error of estimate; SEE) shown by the grey bar. Additionally single clinopyroxene pressure estimates are associated with ± 0.15 GPa SEE and plagioclase-liquid thermobarometry with ± 0.25 GPa SEE [13]. See Supplementary Figure S1 for equilibrium.

The presence of quartz, feldspar and biotite in a single xenolith along with the detrital texture and clay matrix are strong evidence that it is derived from a sedimentary source (Figure 2). It is likely sourced by the sediments that have been deposited on the oceanic plate following ocean crust formation (130–135 Ma [44]). Such sediments are likely to be deep-water pelagic sediments, combined with terrigenous sand derived as windblown dust from the African continental deserts and siliceous to calcareous ooze [45–49].

The mafic lavas from Cape Verde mostly show minimal influence of crustal contamination, traveling rapidly from the lithospheric mantle storage levels through presumably lined magmatic conduits protected from interaction with the surrounding crust [3,15]. More evolved magmas

have crystallized feldspathoids with enriched $\delta^{18}\text{O}$ values and elevated whole rock $\delta^{34}\text{S}$ values [4], this suggests that the feldspathoids and melts are continuing to evolve at shallower levels in the presence of ocean crust and sedimentary contaminants [4]. Hence, the evolved lavas carry signatures of interaction with the upper crust consistent with the presence of crustal xenoliths.

Integrating the information on the crystallization of the lavas and the origin of the xenoliths it is apparent that the lavas crystallize clinopyroxene on storage in the oceanic lithospheric mantle. Subsequently the magmas pass through the oceanic crust and collect xenoliths of oceanic crust gabbro origin (Figure 7). Alternatively, some xenoliths could be wall rock fragments from intermittent crustal magma chambers, for example, [37]. Subsequently during ascent the sedimentary layers are penetrated facilitating the incorporation of occasional sedimentary xenoliths and potentially more subtle influences of crustal contamination prior to ascent through the Cape Verde volcanic pile (Figure 7). This is consistent with the seismic profiles through the Cape Verde region, where 1–2 km of sediment is recorded by low seismic velocities [50] and approximately 1 km of sediments were drilled at the nearby DSDP Site 367 [46].

An interesting aspect is that crustal xenoliths not only occur in lavas from the morphologically young Charles Darwin volcanic field located on comparatively pristine crust but also in the lavas from the mature Cadamosto seamount. However, these two volcanic centres share a predominance of felsic compositions, atypical of Cape Verde, the lower density of felsic magmas may explain the propensity to pool within the crust. This provides evidence that despite of extensive intrusion and potentially lined conduits in the lithosphere beneath a large volcano, the pre-existing crustal lithologies are still accessible to pooled or ascending magma.

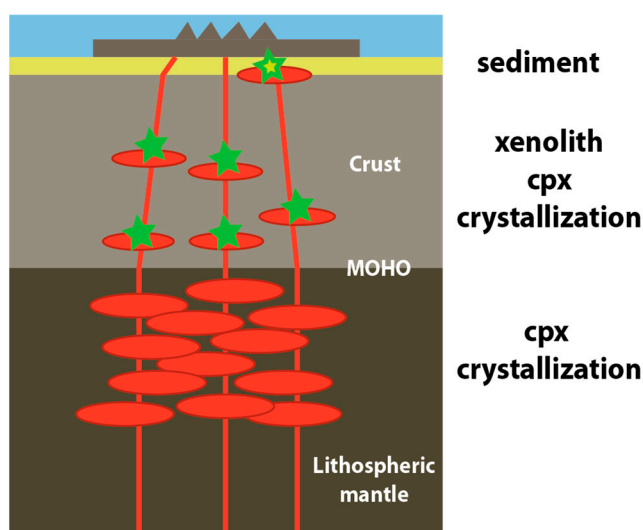


Figure 7. Schematic image of the lithospheric architecture beneath Cape Verde. The lavas crystallize clinopyroxene in the oceanic lithospheric mantle, as they traverse the ocean crust they pick up xenoliths of ocean crust that have crystallized at crustal levels. Subsequently as magma ascent proceeds the magmas cross sediments evidenced by occasional sedimentary xenoliths, before eruption at submarine volcanic centres.

Supplementary Materials: The following are available online at <http://www.mdpi.com/2075-163X/9/2/90/s1>, Figure S1: Mineral-melt equilibrium for clinopyroxene and plagioclase thermobarometry, Table S1: Mineral chemistry data, Table S2: REE in clinopyroxene.

Author Contributions: Sample acquisition, T.H. and A.K.B.; Conceptualization, A.K.B.; Data acquisition; D.N. and A.K.B.; Modelling, A.K.B.; Writing-Original Draft Preparation, A.K.B.; Writing-Review and Editing, A.K.B. and T.H.; Project Administration, A.K.B.; Funding Acquisition, A.K.B.

Funding: This research was funded by the Swedish Research Council (Vetenskapsrådet) grant number Dnr: 2009-4316 and the Swedish Royal Academy of Sciences.

Acknowledgments: We are grateful to the shipboard crew and scientists of the Meteor Expedition M80/3, as well as the Germany Research Council (DFG) for making the sample collection possible. We also thank Hans Harryson and Jarosław Majka for analytical assistance with the electron microprobe analysis at Uppsala University and Matthias Frische for assistance with laser-ablation ICP-MS analyses at GEOMAR. Many thanks to the two reviewers who provided useful insights.

Conflicts of Interest: The authors declare no conflict of interest. The funders had no role in the design of the study; in the collection, analyses or interpretation of data; in the writing of the manuscript and in the decision to publish the results.

References

1. Gerlach, D.C.; Cliff, R.A.; Davies, G.R.; Norry, M.; Hodgson, N. Magma sources of the Cape Verdes archipelago: Isotopic and trace element constraints. *Geochim. Cosmochim. Acta* **1988**, *52*, 2979–2992. [\[CrossRef\]](#)
2. Davies, G.R.; Norry, M.J.; Gerlach, D.C.; Cliff, R.A. A combined chemical and Pb-Sr-Nd isotope study of the Azores and Cape Verde hot-spots: The geodynamic implications. In *Magmatism in Ocean Basins*; Saunders, A.D., Norry, M.J., Eds.; Geological Society of London Special Publication: London, UK, 1989; Volume 42, pp. 231–255.
3. Barker, A.K.; Holm, P.M.; Peate, D.W.; Baker, J.A. Geochemical stratigraphy of submarine lavas (3–5 Ma) from the Flamengos Valley, Santiago, Cape Verde. *J. Petrol.* **2009**, *50*, 169–193. [\[CrossRef\]](#)
4. Barker, A.K.; Troll, V.R.; Ellam, R.M.; Hansteen, T.H.; Harris, C.; Stillman, C.J.; Andersson, A. Magmatic evolution of the Cadamosto Seamount, Cape Verde: Beyond the spatial extent of EM1. *Contrib. Mineral. Petrol.* **2012**, *163*, 949–965. [\[CrossRef\]](#)
5. Bonadiman, C.; Beccaluva, L.; Coltorti, M.; Siena, F. Kimberlite-like metasomatism and ‘garnet signature’ in spinel-peridotite xenoliths from Sal, Cape Verde Archipelago: Relics of a subcontinental mantle domain within the Atlantic oceanic lithosphere? *J. Petrol.* **2005**, *46*, 2465–2493. [\[CrossRef\]](#)
6. Klügel, A. Reactions between mantle xenoliths and host magma beneath La Palma (Canary Islands): Constraints on magma ascent rates and crustal reservoirs. *Contrib. Mineral. Petrol.* **1998**, *131*, 237–257. [\[CrossRef\]](#)
7. Barker, A.K.; Troll, V.R.; Carracedo, J.C.; Nicholls, P. The magma plumbing system for the 1971 Tenguía eruption, La Palma, Canary Islands. *Contrib. Mineral. Petrol.* **2015**, *170*. [\[CrossRef\]](#)
8. Araña, V.; Ibarrola, E. Rhyolitic pumice in the basaltic pyroclasts from the 1971 eruption of Teneguia volcano, Canary Islands. *Lithos* **1973**, *6*, 273–278. [\[CrossRef\]](#)
9. Hansteen, T.H.; Troll, V.R. Oxygen isotope composition of xenoliths from the oceanic crust and volcanic edifice beneath Gran Canaria (Canary Islands): Consequences for crustal contamination of ascending magmas. *Chem. Geol.* **2003**, *193*, 181–193. [\[CrossRef\]](#)
10. Troll, V.R.; Klügel, A.; Longpré, M.A.; Burchardt, S.; Deegan, F.M.; Carracedo, J.C.; Wiesmaier, S.; Kueppers, U.; Dahren, B.; Blythe, L.S.; et al. Floating sandstones off El Hierro (Canary Islands, Spain): The peculiar case of the October 2011 eruption. *Solid Earth* **2012**, *3*, 975–999. [\[CrossRef\]](#)
11. Sigmarsson, O.; Laporte, D.; Carpentier, M.; Devouard, B.; Devidal, J.L.; Marti, J. Formation of U-depleted rhyolite from a basanite at El Hierro, Canary Islands. *Contrib. Mineral. Petrol.* **2013**, *165*, 601–622. [\[CrossRef\]](#)
12. Zaczek, K.; Troll, V.R.; Cachao, M.; Ferreira, J.; Deegan, F.M.; Carracedo, J.C.; Soler, V.; Meade, F.C.; Burchardt, S. Nanofossils in 2011 El Hierro eruptive products reinstate plume model for Canary Islands. *Sci. Rep.* **2015**, *5*, 7945. [\[CrossRef\]](#) [\[PubMed\]](#)
13. Putirka, K. Thermometers and barometers for volcanic systems. *Rev. Mineral. Geochem.* **2008**, *69*, 61–120. [\[CrossRef\]](#)
14. Hildner, E.; Klügel, A.; Hauff, F. Magma storage and ascent during the 1995 eruption of Fogo, Cape Verde Archipelago. *Contrib. Mineral. Petrol.* **2011**, *162*, 751–772. [\[CrossRef\]](#)
15. Hildner, E.; Klügel, A.; Hansteen, T.H. Barometry of lavas from the 1951 eruption of Fogo, Cape Verde Islands: Implications for historic and prehistoric magma plumbing systems. *J. Volcanol. Geotherm. Res.* **2012**, *217*, 73–90. [\[CrossRef\]](#)
16. Ryan, W.B.; Carbotte, S.M.; Coplan, J.O.; O’Hara, S.; Melkonian, A.; Arko, R.; Weissel, R.A.; Ferrini, V.; Goodwillie, A.; Nitsche, F.; et al. Global multi-resolution topography synthesis. *Geochem. Geophys. Geosyst.* **2009**, *10*, 3. [\[CrossRef\]](#)

17. Fietzke, J.; Frische, M. Experimental evaluation of elemental behavior during LA-ICP-MS: Influences of plasma conditions and limits of plasma robustness. *J. Anal. At. Spectrom.* **2016**, *31*, 234–244. [[CrossRef](#)]
18. Jochum, K.P.; Stoll, B.; Herwig, K.; Willbold, M.; Hofmann, A.W.; Amini, M.; Aarburg, S.; Abouchami, W.; Hellebrand, E.; Mocek, B.; et al. MPI-DING reference glass for in situ microanalysis: New reference values for element concentration and isotope ratios. *Geochim. Geophys. Geosyst.* **2006**, *7*, Q02008. [[CrossRef](#)]
19. Jochum, K.P.; Weis, U.; Stoll, B.; Kuzmin, D.; Yang, Q.; Raczek, I.; Jacon, D.E.; Stracke, A.; Birbaum, K.; Frick, D.A.; et al. Determination of reference values for NIST SRM 610–617 Glasses following ISO Guidelines. *Geostand. Geoanal. Res.* **2011**, *35*, 397–429. [[CrossRef](#)]
20. Ashchepkov, I.V.; André, L.; Downes, H.; Belyatsky, B.A. Pyroxenites and megacrysts from Vitim picrite-basalts (Russia): Polybaric fractionation of rising melts in the mantle? *J. Asian Earth Sci.* **2011**, *42*, 14–37. [[CrossRef](#)]
21. Masotta, M.; Mollo, S.; Freda, C.; Gaeta, M.; Moore, G. Clinopyroxene–liquid thermometers and barometers specific to alkaline differentiated magmas. *Contrib. Mineral. Petrol.* **2013**, *166*, 1545–1561. [[CrossRef](#)]
22. Putirka, K.; Ryerson, F.J.; Mikaelian, H. New igneous thermobarometers for mafic and evolved lava compositions, based on clinopyroxene + liquid equilibria. *Am. Mineral.* **2003**, *88*, 1542–1554. [[CrossRef](#)]
23. Putirka, K. Igneous thermometers and barometers based on plagioclase + liquid equilibria: Tests of some existing models and new calibrations. *Am. Mineral.* **2005**, *90*, 336–346. [[CrossRef](#)]
24. Baker, D.R. The fidelity of melt inclusions as records of melt composition. *Contrib. Mineral. Petrol.* **2008**, *156*, 377–395. [[CrossRef](#)]
25. Holm, P.M.; Wilson, J.R.; Christensen, B.P.; Hansen, L.; Hansen, S.L.; Hein, K.H.; Mortensen, A.K.; Pedersen, R.; Plesner, S.; Runge, M.K. Sampling the Cape Verde mantle plume: Evolution of melt compositions on Santo Antão, Cape Verde Islands. *J. Petrol.* **2006**, *47*, 145–189. [[CrossRef](#)]
26. Melson, W.G.; O'Hearn, T. *Smithsonian Volcanic Glass File*; Smithsonian Institution: Washington, DC, USA, 2003.
27. Bougault, H.; Dmitriev, L.V.; Schilling, J.G.; Sobolev, A.V.; Joron, J.-L.; Needham, H.D. Mantle heterogeneity from trace elements: MAR triple junction near 14 N. *Earth Planet. Sci. Lett.* **1988**, *88*, 27–36. [[CrossRef](#)]
28. Duprat, H.I.; Friis, J.; Holm, P.M.; Grandvuinet, T.; Sørensen, R.V. The volcanic and geochemical development of São Nicolau, Cape Verde Islands: Constraints from field and $^{40}\text{Ar}/^{39}\text{Ar}$ evidence. *J. Volcanol. Geotherm. Res.* **2007**, *162*, 1–19. [[CrossRef](#)]
29. Ryabchikov, J.D.; Ntaflos, T.; Kurat, G.; Kogarko, L.N. Glass-bearing xenoliths from Cape Verde: Evidence for a hot rising mantle jet. *Mineral. Petrol.* **1995**, *55*, 217–237. [[CrossRef](#)]
30. Herzberg, C.; Asimow, P.D. Petrology of some oceanic island basalts: PRIMELT2. XLS software for primary magma calculation. *Geochim. Geophys. Geosyst.* **2008**, *9*, Q09001. [[CrossRef](#)]
31. Millet, M.-A.; Doucelance, R.; Schiano, P.; David, K.; Bosq, C. Mantle plume heterogeneity versus shallow-level interactions: A case study, the São Nicolau Island, Cape Verde archipelago. *J. Volcanol. Geotherm. Res.* **2008**, *176*, 265–276. [[CrossRef](#)]
32. Barker, A.K.; Holm, P.M.; Peate, D.W.; Baker, J.A. A five million year record of compositional variations in mantle sources to magmatism on Santiago, southern Cape Verde archipelago. *Contrib. Mineral. Petrol.* **2010**, *160*, 133–154. [[CrossRef](#)]
33. Elkins, L.T.; Grove, T.L. Ternary feldspar experiments and thermodynamic models. *Am. Mineral.* **1990**, *75*, 544–559.
34. Klein, E.M. Geochemistry of the Igneous Oceanic Crust. *Treatise Geochem.* **2004**, *3*, 433–463.
35. Schnetzler, C.C.; Philpotts, J.A. Partition coefficients of rare-earth elements between igneous matrix material and rock-forming mineral phenocrysts; II. *Geochim. Cosmochim. Acta* **1970**, *34*, 331–340. [[CrossRef](#)]
36. Johnson, K.T.M. Experimental determination of partition coefficients for rare earth and high-field-strength elements between clinopyroxene, garnet, and basaltic melt at high pressures. *Contrib. Mineral. Petrol.* **1998**, *133*, 60–68. [[CrossRef](#)]
37. Hansteen, T.H.; Klügel, A.; Schmincke, H.U. Multi-stage magma ascent beneath the Canary Islands: Evidence from fluid inclusions. *Contrib. Mineral. Petrol.* **1998**, *132*, 48–64. [[CrossRef](#)]
38. Kerr, R.C. Convective crystal dissolution. *Contrib. Mineral. Petrol.* **1995**, *121*, 237–246. [[CrossRef](#)]
39. Lofgren, G.E. Effect of heterogeneous nucleation on basaltic textures: A dynamic crystallization study. *J. Petrol.* **1983**, *24*, 229–255. [[CrossRef](#)]
40. Tsuchiyama, A.; Takahashi, E. Melting kinetics of a plagioclase feldspar. *Contrib. Mineral. Petrol.* **1983**, *84*, 345–354. [[CrossRef](#)]

41. Wilson, M. *Igneous Petrogenesis a Global Tectonic Approach*, 1st ed.; Chapman and Hall: London, UK, 1989.
42. Doucelance, R.; Escrig, S.; Moriera, M.; Gariepy, C.; Kurz, M. Pb-Sr-He isotope and trace element geochemistry of the Cape Verde Archipelago. *Geochim. Cosmochim. Acta* **2003**, *67*, 3717–3733. [[CrossRef](#)]
43. Lodge, A.; Helffrich, G. Depleted swell root beneath the Cape Verde Islands. *Geology* **2006**, *34*, 449–452. [[CrossRef](#)]
44. Ali, M.Y.; Watts, A.B.; Hill, I.A. seismic reflection profile study of lithospheric flexure in the vicinity of the Cape Verde Islands. *J. Geophys. Res.* **2003**, *108*, 2239–2263. [[CrossRef](#)]
45. Lancelot, Y.; Seibold, E.; Cepek, P.; Dean, W.E.; Eremeev, V.; Gardner, J.; Jansa, L.F.; Johnson, D.; Krasheninnikov, V.; Pflaumann, U.; et al. DSDP Site 367: Cape Verde Basin. *DSDP Initial Rep.* **1978**, *151*. [[CrossRef](#)]
46. Hoernle, K.; Tilton, G.; Schminke, H.U. Sr-Nd-Pb isotopic evolution of Gran Canaria: Evidence for shallow enriched mantle beneath the Canary Islands. *Earth Planet. Sci. Lett.* **1991**, *106*, 44–63. [[CrossRef](#)]
47. Grouset, F.E.; Parra, M.; Bory, A.; Martinez, P.; Bertrand, P.; Shimmield, G.; Ellam, R. Saharan wind regimes traced by the Sr-Nd isotopic composition of subtropical Atlantic sediments: Last Glacial maximum vs. today. *Quat. Sci. Rev.* **1998**, *17*, 395–409. [[CrossRef](#)]
48. Abouchami, W.; Galer, S.J.G.; Koschinsky, A. Pb and Nd isotopes in NE Atlantic Fe-Mn crusts: Proxies for trace metal paleosources and paleocean circulation. *Geochim. Cosmochim. Acta* **1999**, *63*, 1489–1505. [[CrossRef](#)]
49. Samrock, L.K.; Dullo, W.C.; Hansteen, T.H. Large-scale fossil dune on Maio, Cape Verdes. *Int. J. Earth Sci.* **2018**, *107*, 2931–2932. [[CrossRef](#)]
50. Pim, J.; Peirce, C.; Watts, A.B.; Grevemeyer, L.; Krabbenhoft, A. Crustal structure and origin of the Cape Verde Rise. *Earth Planet. Sci. Lett.* **2008**, *272*, 422–428. [[CrossRef](#)]



© 2019 by the authors. Licensee MDPI, Basel, Switzerland. This article is an open access article distributed under the terms and conditions of the Creative Commons Attribution (CC BY) license (<http://creativecommons.org/licenses/by/4.0/>).